

# Improving Triplet-Based Channel Charting on Distributed Massive MIMO Measurements

Florian Euchner, Phillip Stephan, Marc Gauger, Sebastian Dörner, Stephan ten Brink  
Institute of Telecommunications, Pfaffenwaldring 47, University of Stuttgart, 70569 Stuttgart, Germany  
{euchner,stephan,gauger,doerner,tenbrink}@inue.uni-stuttgart.de

**Abstract**—The objective of channel charting is to learn a virtual map of the radio environment from high-dimensional channel state information (CSI) that is acquired by a multi-antenna wireless system. Since, in static environments, CSI is a function of the transmitter location, a mapping from CSI to channel chart coordinates can be learned in a self-supervised manner using dimensionality reduction techniques. The state-of-the-art triplet-based approach is evaluated on multiple datasets measured by a distributed massive multiple-input multiple-output (MIMO) channel sounder, with both co-located and distributed antenna setups. The importance of suitable triplet selection is investigated by comparing results to channel charts learned from a genie-aided triplet generator and learned from triplets on simulated trajectories through measured data. Finally, the transferability of learned forward charting functions to similar, but different radio environments is explored.

## I. INTRODUCTION

Motivated by ever increasing wireless traffic volumes, spatial multiplexing through massive multiple-input multiple-output (MIMO) has been identified as a crucial technology for improving spectral efficiency. With massive MIMO, which requires a large number of antennas at the base station (BS), the number of channel estimates necessary for communication over the channel between BS and user equipment (UE) has increased. Acquired channel estimates, which can be expressed in various representations (e.g., in frequency domain or in time domain), are commonly referred to as channel state information (CSI). Collecting CSI, which necessarily arises at the BS, opens the door for many data-driven applications, including localization of UEs. Successful supervised learning experiments have established that localization based on CSI fingerprinting is possible in principle [1] [2] [3] [4] [5]. However, any supervised learning technique requires accurate UE position labels for training, which are usually not available. Self-supervised training methods, which do not require ground truth position labels, are therefore an attractive alternative.

Channel charting, originally proposed by C. Studer et al. [6], is one such self-supervised technique that aims to learn a mapping from the high-dimensional space of possible CSI vectors to a low-dimensional space, the so-called channel chart. The channel chart is supposed to maintain the local geometry of the radio environment. Depending on the application, it may be desirable to be able to map the chart back to physical space, or the channel chart may be useful in and of itself.

As shown in Fig. 1, the key steps in channel charting, apart from acquiring a large CSI dataset, are feature engineering

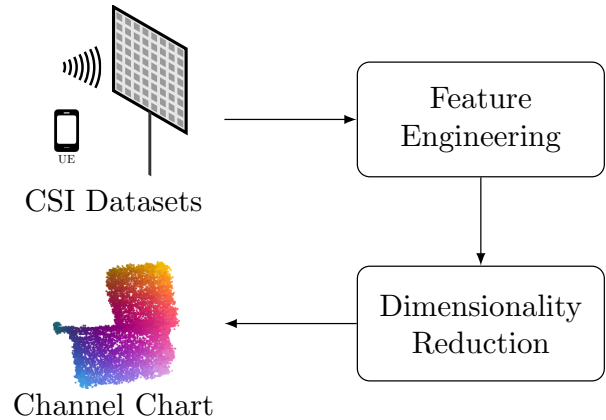


Fig. 1: Overview of the Channel Charting Pipeline

and dimensionality reduction. In a practical system, large CSI datasets could be obtained at the BS from multiple UEs over a long timespan. Despite CSI being abundant in real-world massive MIMO systems, most of the research currently published is based on synthetic data. Trials on real-world measurements, on the other hand, are rare and perform poorly in comparison [7]. This raises the question of whether this is due to the available amount of data, due to properties of real-world datasets or a result of shortcomings of the current feature engineering or dimensionality reduction methods. We aim to help address this question by making the following contributions:

- With our channel sounder, we measure large CSI datasets, which are made publicly available<sup>1</sup>, and apply state-of-the-art triplet neural network-based channel charting, as defined in Section II, to the data.
- We introduce genie-aided and partially genie-aided baselines for triplet selection to benchmark time-based triplet selection against and compare the performance of these different selection rules for dense neural network (DNN) training in Section IV.
- We test the transferability of learned channel mappings to different datasets for same and similar, but different environments in Section V.

<sup>1</sup>Datasets and a tutorial for a special case of channel charting is available at <https://dichasus.inue.uni-stuttgart.de/tutorials/tutorial/channelcharting/>

## II. STATE-OF-THE-ART CHANNEL CHARTING OVERVIEW

### A. System Model

We consider a wireless transmission system consisting of a massive MIMO BS with  $B$  antennas and a single-antenna transmitter. At the BS, CSI for  $W$  orthogonal frequency division multiplex (OFDM) subcarriers is collected at each time instant  $n = 1, \dots, N$  for different UE positions  $\mathbf{x}_n \in \mathbb{R}^D$ , with  $D$  being the physical spatial dimensionality. CSI for a particular time instant can be expressed either as a matrix of channel coefficients  $\mathbf{S}_n \in \mathbb{C}^{B \times W}$ , or in its vectorized representation  $\mathbf{h}_n = \text{vec}(\mathbf{S}_n) \in \mathbb{C}^M$ , with  $M = B \cdot W$ . As part of a feature engineering stage  $\mathcal{F} : \mathbb{C}^M \rightarrow \mathbb{C}^{M'}$ , the CSI vector is transformed into a feature vector  $\mathbf{f}_n \in \mathbb{R}^{M'}$ .

Channel charting is a dimensionality reduction technique, with the objective of finding a *forward charting function*

$$\mathcal{C} : \mathbb{C}^{M'} \rightarrow \mathbb{R}^{D'},$$

which maps points from feature space to the  $D'$ -dimensional channel chart (here:  $D' = 2$ ). Charts are generated from a dataset made up of datapoints that are 3-tuples of channel coefficients  $\mathbf{S}_n$ , UE positions  $\mathbf{x}_n \in \mathbb{R}^D$  and timestamps  $t_n$ :

$$\text{Dataset: } \{(\mathbf{S}_n, \mathbf{x}_n, t_n)\}_{n=1, \dots, N}$$

### B. Feature Engineering

The main purpose of feature engineering is to extract large-scale fading characteristics from CSI. In this work, we adopt the *scaled raw 2<sup>nd</sup> moment (R2M)* representation  $\mathbf{H} \in \mathbb{C}^{M \times M}$  as originally defined in [4] (including their notation), and choose the estimated path loss exponent to be  $\sigma = 8$ . Here, the feature vector  $\mathbf{f}_{n, \text{cplx}}$  is the vectorized form of  $\mathbf{H}$ , i.e.  $\mathbf{f}_{n, \text{cplx}} = \text{vec}(\mathbf{H}) \in \mathbb{C}^{M^2}$  and  $M' = M^2$ . Experiments on our datasets suggest that using either only real or only imaginary parts of  $\mathbf{f}_{n, \text{cplx}}$  yields a performance comparable to using complex-valued R2M. Therefore, and for complexity reasons, we chose the final feature vector to be  $\mathbf{f}_n = \Re\{\mathbf{f}_{n, \text{cplx}}\}$ .

### C. Forward Charting Function

The forward charting function  $\mathcal{C}$  can either be implemented as a conventional dimensionality reduction technique or as a trainable DNN. By realizing  $\mathcal{C}$  as a DNN, once trained, new CSI datapoints can be mapped to the channel chart with low computational complexity, which is highly desirable. The DNN may be trained using an autoencoder structure [6], as part of a siamese network [8] or using triplet loss [9]. We will focus on the last, which appears to be most promising.

Furthermore, charting functions can be learned either *purely* based on CSI, or based on CSI and timestamps: Without relying on ground truth position labels, it is difficult to tell whether two CSI samples are close to each other in physical space or not. However, based on the assumption that samples measured close in time are likely to be close in space as well, [9] proposes to select triplets based on timestamps, which are almost certainly available at any BS. Since the availability of timestamp labels does not pose a challenge for practical systems, we will focus on training techniques which do take time into account.

### D. Triplet loss-based DNN training

Figuratively speaking, a charting function  $\mathcal{C}$  is good if it preserves the local and global geometry of real space except for rotations and/or scalings: Datapoints that are close to each other in physical space should also be close in the channel chart (and vice versa for distant datapoints). This motivates training with triplet loss, where the DNN  $\mathcal{C}$  learns from *positive* (similar) and *negative* (dissimilar) examples [9]. For training, three CSI vectors measured at physical locations ( $\mathbf{x}_{\text{anchor}}, \mathbf{x}_{\text{pos}}, \mathbf{x}_{\text{neg}}$ ) are required. This triplet consists of the anchor point  $\mathbf{x}_{\text{anchor}}$ , the positive sample  $\mathbf{x}_{\text{pos}}$  and the negative sample  $\mathbf{x}_{\text{neg}}$ . For the subsequent investigations, it is important to know that  $\mathbf{x}_{\text{anchor}}, \mathbf{x}_{\text{pos}}$  and  $\mathbf{x}_{\text{neg}}$  should fulfill

$$\|\mathbf{x}_{\text{anchor}} - \mathbf{x}_{\text{pos}}\| \leq \|\mathbf{x}_{\text{anchor}} - \mathbf{x}_{\text{neg}}\|. \quad (1)$$

Finding such triplets is the subject of *triplet selection*.

1) *Triplet Selection*: To generate a set of — in our case 1 200 000 — triplets to train the DNN on, an anchor datapoint ( $\mathbf{S}_{\text{anchor}}, \mathbf{x}_{\text{anchor}}, t_{\text{anchor}}$ ) is drawn from the dataset for each triplet. Then, a datapoint ( $\mathbf{S}_{\text{pos}}, \mathbf{x}_{\text{pos}}, t_{\text{pos}}$ ) is randomly chosen out of the set of datapoints ( $\mathbf{S}_n, \mathbf{x}_n, t_n$ ) for which  $|t_n - t_{\text{anchor}}| \leq T_c$ , where  $T_c$  is a threshold interval for positive samples. Unless otherwise specified, we will assume  $T_c = 1.5$  s. Next, the negative sample ( $\mathbf{S}_{\text{neg}}, \mathbf{x}_{\text{neg}}, t_{\text{neg}}$ ) is randomly drawn from the entire dataset. We found that imposing a restriction on the negative sample such as  $|t_{\text{neg}} - t_{\text{anchor}}| > T_c$  does not lead to better channel charts, most likely since it is probable that the restriction is fulfilled anyway. All random selections are performed with uniform probability. Note that Eq. (1) is likely to be fulfilled by this triplet choice, but it is not guaranteed to be.

2) *Neural Network Training*: Our neural network architecture and loss function are identical to [9, Section VI.B]. The DNN  $\mathcal{C}$  is trained by feeding positive, negative and anchor sample into three separate DNNs  $\mathcal{C}$  with weight sharing and using triplet loss with margin  $M = 1$ .

### E. Performance Metrics for Channel Charting

Throughout this work, we will repeatedly evaluate channel charts on three performance metrics commonly used in channel charting literature [6] [8]:

- **Continuity (CT)** and **Trustworthiness (TW)** [10] are two measures, normalized to the range  $[0, 1]$ , for the preservation of *local* neighborhoods. Figuratively speaking, a high CT indicates that many neighborhood relationships in physical space are preserved in the channel chart. A high TW value, on the other hand, indicates that the channel chart does not contain many additional false neighborhood relationships, i.e., ones which are not present in physical space. We use CT and TW as defined in [6] and adopt  $K = 0.05 \cdot N$  as neighborhood size.
- **Kruskal Stress (KS)**, first applied to channel charting in [11], is a measure for the preservation of the global channel chart structure. It is also bounded to range  $[0, 1]$ , with 0 indicating the best and 1 indicating the worst possible performance. We adopt the scaling from [9].

### III. MEASURED DATASETS

We analyze three datasets captured by our channel sounder called Distributed Channel Sounder by University of Stuttgart (DICHASUS), with a carrier frequency of 1.272 GHz,  $W = 1024$  OFDM subcarriers and a bandwidth of 50 MHz:

- **Indoor:** Subset of *dichasus-015x* [12] with  $N = 13496$  datapoints, measured in an indoor office environment with a single  $B = 32$ -antenna uniform planar array. The transmitter moves along a meandering trajectory.
- **Distributed:** Subset of *dichasus-0d5x* [13] with  $N = 22332$  datapoints, measured in the same indoor environment as the “Indoor” dataset, but with two separate 16-antenna uniform planar arrays ( $B = 32$  in total). The transmitter moves along a meandering trajectory.
- **Industrial:** Subset of *dichasus-cb0x* [14] with  $N = 19919$  datapoints, measured in a factory building with a single antenna array, with data from  $B = 21$  antennas in the dataset. The transmitter moves along different meandering and pseudorandom trajectories with high speed.

To reduce computational cost and in contrast to Section II-B, only a mean value, computed over the channel coefficients of 8 subcarriers in the center of the band, is used for  $\mathbf{h}_n$ :

$$[\mathbf{h}_n]_b = \frac{1}{8} \sum_{w=508}^{515} [\mathbf{S}_n]_{b,w},$$

where  $[\mathbf{S}_n]_{b,w}$  denotes the channel coefficient measured by antenna  $b$  on subcarrier  $w$ . We continue with Feature Engineering as explained in Section II-B, mapping  $\mathbf{h}_n \in \mathbb{C}^B$  to the feature vector  $\mathbf{f}_n \in \mathbb{C}^{B^2}$  that is provided to the DNN for training and evaluation, as explained in Section II. The ground truth position labels and resulting channel charts for all datasets are shown in Fig. 2 in the first and second rows, respectively. All charts, judging by performance metrics and appearance, are acceptable, but fail to learn the global geometry. For example, the rectangular shapes in the ground truth are not recognizable in the channel charts. In the following, we will show that, without changing the training procedure, performance could be significantly improved through better triplet selection.

### IV. TRIPLET GENERATION

Triplet selection in state-of-the-art channel charting is time-based and therefore dependent on the particular trajectory taken by the UE. To understand if different trajectories would have yielded better channel charts with the same DNN training technique, we can leverage the ground truth position labels contained in DICHASUS datasets. We compare an idealized genie-aided triplet selection technique to a method based on large numbers of simulated (but realistic) trajectories.

#### A. Distance-Based Triplet Selection (Genie-Aided)

Triples are selected by randomly drawing an anchor point  $(\mathbf{S}_{\text{anchor}}, \mathbf{x}_{\text{anchor}}, t_{\text{anchor}})$  and negative sample  $(\mathbf{S}_{\text{neg}}, \mathbf{x}_{\text{neg}}, t_{\text{neg}})$  from the whole dataset and a positive sample from the set of all datapoints  $(\mathbf{S}_n, \mathbf{x}_n, t_n)$  for which

$\|\mathbf{x}_n - \mathbf{x}_{\text{anchor}}\| \leq d_c$ , where  $d_c$  is the maximum spatial distance between anchor point and positive sample. All random selections are made with uniform probability. Experiments have shown that imposing  $\|\mathbf{x}_{\text{anchor}} - \mathbf{x}_{\text{neg}}\| > d_c$  as an additional restriction only marginally improves performance. It was found that  $d_c = 1.5$  m is a good choice for the “Indoor” dataset with regards to the performance metrics, as illustrated in Fig. 3. The resulting channel charts, shown in the third row of Fig. 2, demonstrate that local and global geometry is preserved when training on genie-generated triplets.

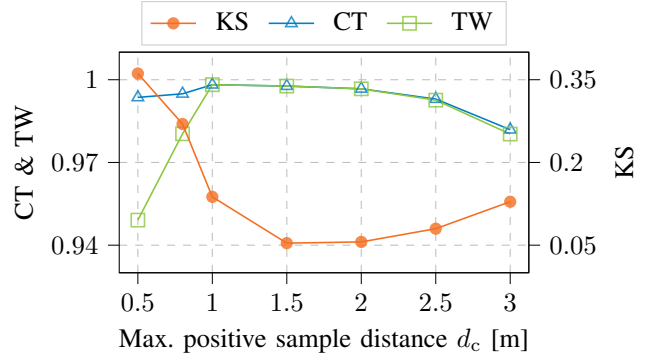


Fig. 3: Performance metrics as a function of  $d_c$ , genie-aided triplet selection evaluated on “Indoor” dataset

#### B. Time-Based Triplet Selection on Simulated Trajectories

A set of  $r$  simulated, but realistic UE trajectories with constant velocity  $v = 1$  m/s through the dataset is generated and triplets are drawn from this set according to the state-of-the-art time-based triplet selection with  $T_c = 1.5$  s. This is best explained with Fig. 4a, where four exemplary simulated trajectories were generated (black), anchor (red) and positive sample (blue) were randomly drawn within  $T_c$  on the same trajectory, and the negative sample (green) is chosen from a random trajectory. We only consider disjoint straight lines as potential trajectories, experiments with other trajectory shapes such as Bézier curves did not yield any performance improvements. Compared to triplet selection based on the UE’s real trajectory, using simulated trajectories makes it possible to remove biases introduced during data acquisition (e.g., meandering UE paths) and to better understand desirable properties of trajectories. For large numbers of simulated trajectories ( $r \rightarrow \infty$ ), time-based selection on simulated trajectories becomes similar (but never identical) to genie-aided triplet selection.

With  $r = 30000$ , performance comparable to genie-aided triplet selection is achievable as shown in the fourth row of Fig. 2, except for the “Industrial” dataset. Datapoints in that dataset are spread over a larger area, thus setting  $T_c = 3$  improves the result significantly, as illustrated in Fig. 4b. For the other datasets, the results are almost as good as those produced with genie-aided triplet selection. Fig. 4c, which was generated based on the “Indoor” dataset, shows that channel charting performance is highly dependent on the number of simulated trajectories. We conclude that a dataset which contains a large variety of paths is essential for channel charting.

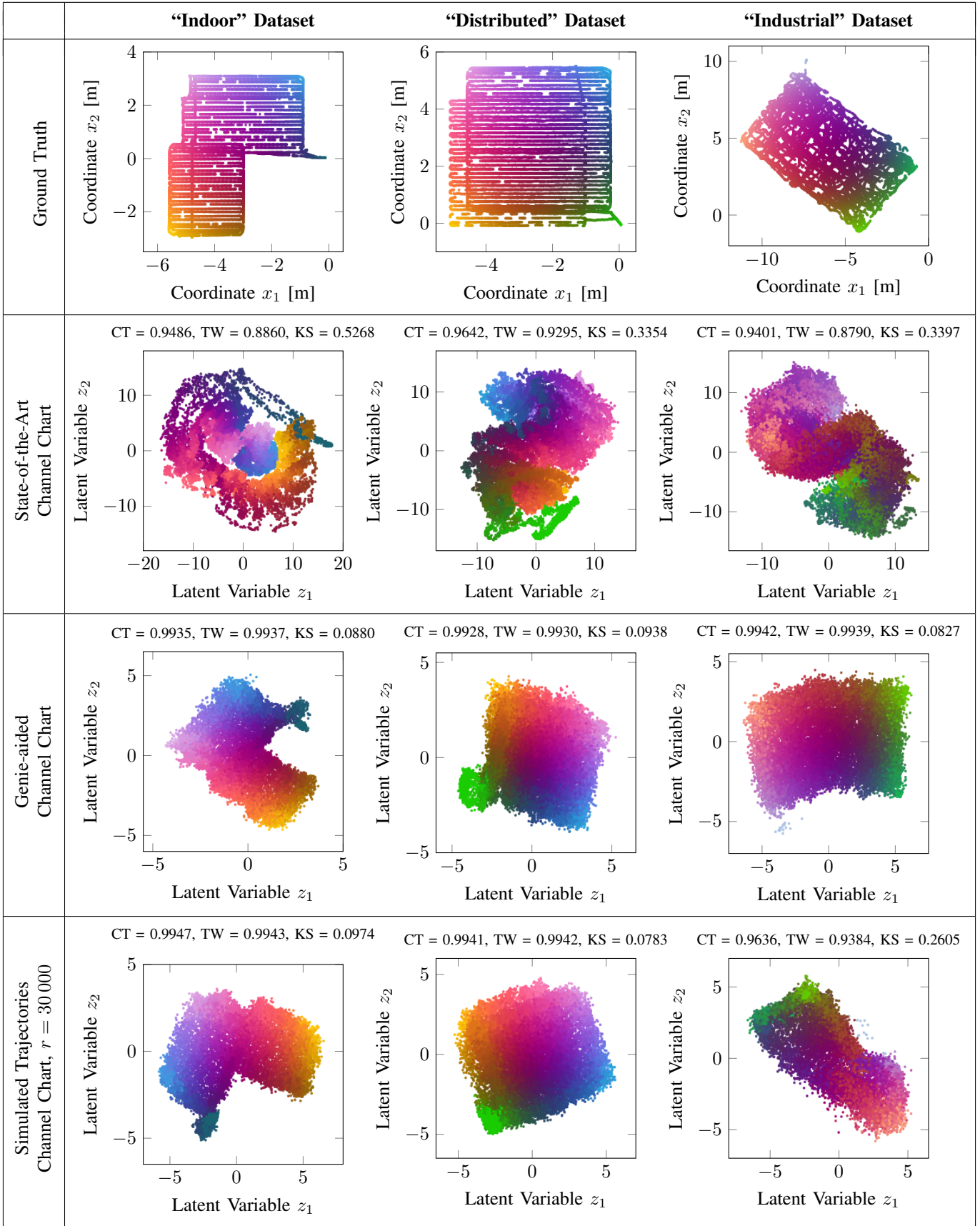
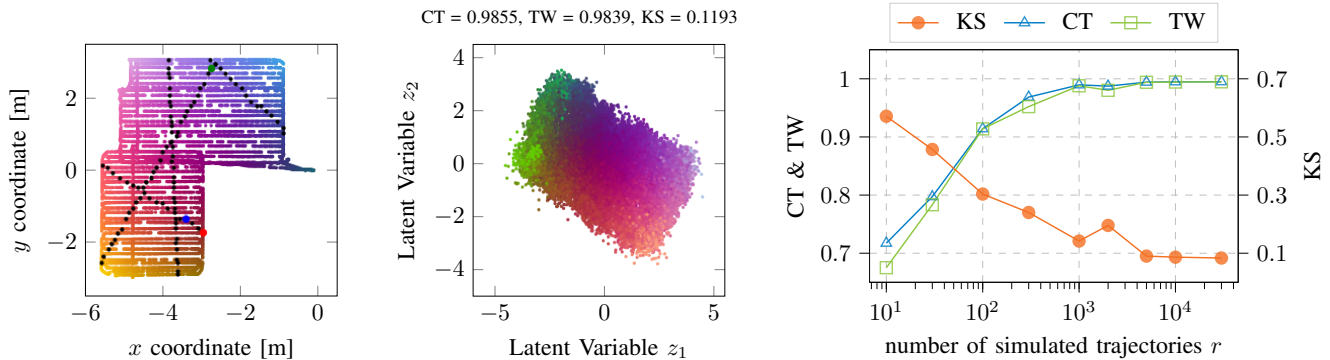


Fig. 2: Colored ground truth positions and different channel charts (with colorings preserved) including performance metrics generated from CSI: Computed with “state-of-the-art” method, genie-aided triplet generation and from simulated trajectories.





(a) Conceptual illustration of simulated trajectories (“Indoor” dataset) (b) Simulated trajectories channel chart, “Industrial” dataset,  $T_c = 3$  (c) Performance as a function of the number of simulated trajectories, evaluated on “Indoor” dataset

Fig. 4: Several illustrations pertaining the use of simulated trajectories for triplet generation

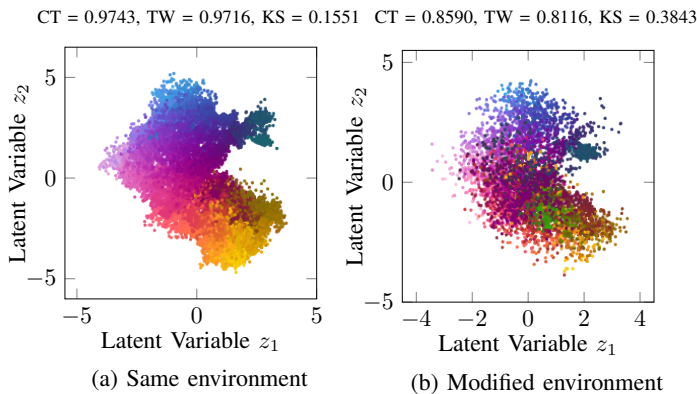


Fig. 5: Transferred channel charts:  $\mathcal{C}$  is evaluated on different datasets after training on the “Indoor” dataset

## V. TRANSFERRING CHANNEL CHARTS

We apply the forward charting function  $\mathcal{C}$  previously learned for the “Indoor” dataset after genie-aided triplet selection (Fig. 2, third row, first column) to different, previously unseen data. Fig. 5a shows the channel chart obtained by applying  $\mathcal{C}$  to a CSI dataset captured in the exact same radio environment at a later point in time. Despite having never seen any datapoint from this set,  $\mathcal{C}$  can still extract the local and global geometry. In another experiment,  $\mathcal{C}$  is evaluated on a different dataset in a similar environment, but with an additional obstacle in the line-of-sight path [15]. As illustrated in Fig. 5b,  $\mathcal{C}$  still recognizes contiguous regions, but performance is degraded.

## VI. SUMMARY AND OUTLOOK

We have successfully applied triplet-based channel charting to multiple datasets acquired by a massive MIMO channel sounder. We investigated the importance of triplet selection and showed the possibility of transferring learned forward charting functions to unseen data. The transferability of channel charts to new data motivates a potential pre-training of the DNN that implements the forward charting function on model-generated data, as in [5]. With this paper, we highlight the importance of large and varied training datasets and provide a

framework for evaluating neural network training techniques independent of the true UE trajectory.

## REFERENCES

- [1] V. Savić and E. G. Larsson, “Fingerprinting-based positioning in distributed massive MIMO systems,” in *2015 IEEE 82nd vehicular technology conference (VTC2015-Fall)*. IEEE, 2015, pp. 1–5.
- [2] J. Vieira, E. Leitinger, M. Sarajlic, X. Li, and F. Tufvesson, “Deep convolutional neural networks for massive MIMO fingerprint-based positioning,” in *2017 IEEE 28th Annual International Symposium on Personal, Indoor, and Mobile Radio Communications (PIMRC)*. IEEE, 2017, pp. 1–6.
- [3] M. Arnold, J. Hoydis and S. ten Brink, “Novel Massive MIMO Channel Sounding Data Applied to Deep Learning-based Indoor Positioning,” *SCC 2019*, Feb. 2019.
- [4] P. Ferrand, A. Decurninge, and M. Guillaud, “DNN-based Localization from Channel Estimates: Feature Design and Experimental Results,” *CoRR*, vol. abs/2004.00363, 2020.
- [5] M. Arnold, S. Dörner, S. Cammerer, and S. ten Brink, “On Deep Learning-based Massive MIMO Indoor User Localization,” 2018.
- [6] C. Studer, S. Medjkouh, E. Gönültaş, T. Goldstein, and O. Tirkkonen, “Channel Charting: Locating Users within the Radio Environment using Channel State Information,” *CoRR*, vol. abs/1807.05247, 2018.
- [7] B. Rappaport, E. Gönültaş, J. Hoydis, M. Arnold, P. K. Srinath, and C. Studer, “Improving Channel Charting using a Split Triplet Loss and an Inertial Regularizer,” in *2021 17th International Symposium on Wireless Communication Systems (ISWCS)*. IEEE, 2021, pp. 1–6.
- [8] E. Lei, O. Castañeda, O. Tirkkonen, T. Goldstein, and C. Studer, “Siamese Neural Networks for Wireless Positioning and Channel Charting,” 2019.
- [9] P. Ferrand, A. Decurninge, L. G. Ordoñez, and M. Guillaud, “Triplet-Based Wireless Channel Charting: Architecture and Experiments,” *IEEE Journal on Selected Areas in Communications*, vol. 39, no. 8, 2021.
- [10] J. Venna and S. Kaski, “Neighborhood preservation in nonlinear projection methods: An experimental study,” in *International Conference on Artificial Neural Networks*. Springer, 2001, pp. 485–491.
- [11] P. Huang, O. Castañeda, E. Gönültaş, S. Medjkouh, O. Tirkkonen, T. Goldstein, and C. Studer, “Improving channel charting with representation-constrained autoencoders,” in *2019 IEEE 20th International Workshop on Signal Processing Advances in Wireless Communications (SPAWC)*. IEEE, 2019, pp. 1–5.
- [12] F. Euchner and M. Gauger, “CSI Dataset dichasus-015x: Indoor Line of Sight, Lab Room,” 2021. [Online]. Available: <https://doi.org/doi:10.18419/darus-2202>
- [13] —, “CSI Dataset dichasus-0d5x: Distributed Arrays: Indoor LoS, Lab Room,” 2021. [Online]. Available: <https://doi.org/doi:10.18419/darus-2218>
- [14] —, “CSI Dataset dichasus-cb0x: Industrial Environment LoS Day 2,” 2022. [Online]. Available: <https://doi.org/doi:10.18419/darus-2604>
- [15] —, “CSI Dataset dichasus-005x: Indoor Non-Line of Sight, Single Room,” 2021. [Online]. Available: <https://doi.org/doi:10.18419/darus-2204>